Article

Hydrogen-Bond Topology Is More Important Than Acid/Base Strength in Atmospheric Prenucleation Clusters

Shannon E. Harold, Conor J. Bready, Leah A. Juechter, Luke A. Kurfman, Sara Vanovac, Vance R. Fowler, Grace E. Mazaleski, Tuguldur T. Odbadrakh, and George C. Shields*

Read Online

ACCESS | Metrics & More | Article Recommendations | Supporting Information

ABSTRACT: We explored the hypothesis that on the nanoscale level, acids and bases might exhibit different behavior than in bulk solution. Our study system consisted of sulfuric acid, formic acid, ammonia, and water. We calculated highly accurate Domain-based Local pair-Natural Orbital- Coupled-Cluster/Complete Basis Set (DLPNO-CCSD(T)/CBS) energies on DFT geometries and used the resulting Gibbs free energies for cluster formation to compute the overall equilibrium constants for every possible cluster. The equilibrium constants combined with the initial monomer concentrations were used to predict the formation of clusters at the top and the bottom of the troposphere. Our results show that formic acid is as effective as ammonia at forming clusters with sulfuric acid and water. The structure of formic acid is uniquely suited to form hydrogen bonds with sulfuric acid.

Additionally, it can partner with water to form bridges from one side of sulfuric acid to the other, hence demonstrating that hydrogen bonding topology is more important than acid/base strength in these atmospheric prenucleation clusters.
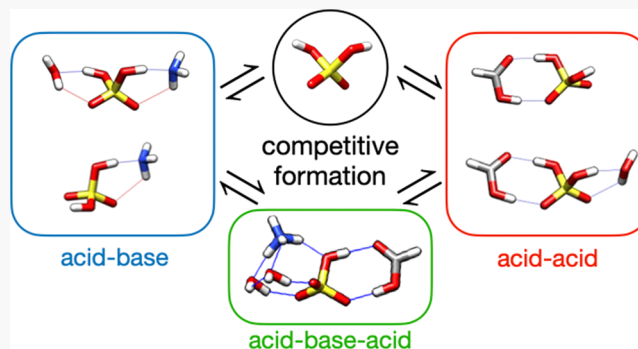
INTRODUCTION

Atmospheric aerosols or particulate matter derived from both natural and anthropogenic sources have been widely studied because of their important environmental impacts. Currently, they are thought to have a net cooling effect on the atmosphere.[1] Aerosols are known to affect the climate in several ways including by light scattering, absorbing and emitting thermal radiation, and serving as cloud condensation nuclei (CNN).[2] Heavy dust aerosols absorb blue wavelengths; however, brighter aerosols, such as those containing sulfates, reflect sunlight away from the earth.[3] Additionally, evidence points to a strong relationship between aerosols and extreme weather events including heavy rainfall and deep convection in the tropics.[4]

Aerosols come from a variety of sources and are classified as primary and secondary aerosols. Primary aerosols are emitted into the air as preexisting particles and include things like soot and pollen. Secondary aerosols are formed in the air by reactions within clusters of gas-phase molecules.[5] The formation of these aerosols and their detailed effects on the atmosphere are not well understood, presenting a gap in our understanding of climate change. Different molecules come together in the atmosphere and under favorable conditions will grow into larger gas-phase clusters and nanometer-sized aerosol particles, a process known as new particle formation (NPF).[6] These particles can continue to grow under certain conditions into CCN or ice nuclei (IC) that act as the initial site for the condensation of water droplets. A holistic understanding of this process requires an investigation of the initial gas-phase clusters in the atmosphere that serve as precursors to larger aerosols, yet current state-of-the-art experimental techniques have difficulties in accessing the entire size range, from subnanometer to 10 nm, consistently. Every size regime requires a mass spectrometer that works at that size, which makes it difficult to draw conclusions from all the data.[7,8]

Past studies have established the role of sulfuric acid as a strong nucleator of CCN.[9−11] Atmospheric sulfuric acid is formed in the two-step process, oxidation of SO_2 followed by hydration of SO_3.[12−14] The main sources of SO_2 are fossil fuel combustion and industrial processes, biomass burning, and volcanic plumes.[15] Interestingly, formic acid has been shown to catalyze the hydration of SO_3 to aid in the formation of atmospheric sulfuric acid, which in turn can undergo stabilizing acid−base reactions with amines and organic acids,[16] as well as
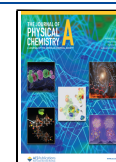
formic acid itself.[9,14,17] In this way, sulfuric acid maintains an atmospheric concentration range of 10^5 to 10^8 cm^{-3}.[9]

The two-component sulfuric acid−water system has been extensively studied using computational methods,[8] as well as with electronic structure methods that include electron correlation.[9,10,18−22] The ammonia−sulfuric acid system has also been studied extensively.[23−27] The sulfuric acid−ammonia−water system is perhaps the most studied system[8] as ammonia has ppb concentrations in the atmosphere[28] and has also been comprehensively studied with electron correlation methods.[19,20,29−36]

Formic acid has been less studied.[37−39] Nadykto and Yu used the density functional theory (DFT) method, PW91PW91, with a triple zeta basis set and compared the sulfuric acid−formic acid−water and sulfuric acid−acetic acid−water systems to the sulfuric acid−ammonia−water system. They concluded that the stabilizing effect of formic acid and acetic acid is close to that of ammonia, indicating that these organics may efficiently stabilize small H_2SO_4−H_2O clusters. They recommended that the involvement of formic and acetic acids in atmospheric nucleation be studied further.[40]

Formic acid is relatively abundant with concentrations spanning from 2.46×10^9 to 1.62×10^{11} cm^{-3}.[41−43] It stems from a series of reactions with isoprene as well as other anthropogenic and natural sources, such as vegetation.[42,43] Surprisingly, the high concentration of formic acid cannot be explained by our current understanding of production and loss pathways, and there seem to be hidden pathways for formic acid production in the atmosphere.[42,43]

Ammonia has a high atmospheric concentration of 5.2×10^8 to 2.46×10^{11} cm^{-3}.[28,44−46] In rural areas, the highest amounts of ammonia are emitted into the atmosphere from agricultural activities, such as fertilization and livestock volatilization.[44]

Large aerosols consist of many numbers of acids and bases, and field-based evidence suggested that bases enhance nucleation via one-to-one acid−base pairs that stabilize these clusters.[47,48] Previous studies suggested that the stabilizing effects of acid−base interactions in atmospheric prenucleation clusters can be correlated to the acid/base strengths of the involved species.[49] "Diagonal" acid−base pairs were studied because approximately equal numbers of acids and bases are thought to be the most stable.[50] Synergistic effects between different bases can greatly enhance sulfuric acid−base cluster formation.[24,51] As the clusters become more complex, studying hydration becomes computationally expensive, which is why most studies avoid including water for large multicomponent clusters.[8] However, water clusters are important in atmospheric chemistry.[52−61] Recently, laboratory studies have shown that acid−base particles with mobility diameters in the range of 5 to 7 nm are acidic, with acid/base ratios as high as 1.8, but reverting to 1 at around 12 nm.[62,63]

Our goal was to examine the hypothesis that on the nanoscale level, acids and bases exhibit different behaviors than what is observed for bulk aerosols. We picked the formic acid−sulfuric acid−ammonia system for this study. We computed every possible combination of each of these three molecules, including a small number of water molecules. Varying numbers of water molecules (0−5) were added to each cluster to predict the number of waters that create the most stable clusters and to visualize how the waters interact with each component of the cluster. Assuming 100% humidity, water has an atmospheric concentration of 7.7×10^{17} cm^{-3} at 298 K at

the bottom of the troposphere and 9.9×10^{14} cm^{-3} at 217 K at the top of the troposphere.[28]

The structural and energetic results from our study led to the fascinating conclusion that hydrogen bonding topology could be more important than acid and base strength at the nanoscale level. In particular, formic acid is an ideal hydrogen bonding partner with sulfuric acid and interactions between sulfuric acid, formic acid, and water are just as strong as interactions between sulfuric acid, ammonia, and water. By looking at all the different conformers made from these components and calculating their free energies, we gained insights into the stability of these clusters that help us understand how prenucleation complexes eventually form aerosols.

■ METHODOLOGY

We define our total system as the gas-phase equilibrium between infinitely separated monomers of sulfuric acid (SA), formic acid (FA), ammonia (A), and water (w) and all possible combinations of bound and hydrated clusters for $n = 0−5$. This can be written as a set of coupled equilibria, where each reaction consists of either the formation of a dry dimer or trimer cluster or the addition of one water molecule to an already formed cluster. These can then be solved for the equilibrium concentrations of all species using the Gibbs free energy changes of these individual reactions.[64] Therefore, the computation of the equilibrium concentrations of the species involves (1) the identification of the most stable geometries of the isolated monomers SA, FA, A, and w, (2) the identification of the most stable geometries of the bound gas-phase clusters SAw_n, FAw_n, Aw_n, SA(FA)w_n, SA(A)w_n, FA(A)w_n, and SA(FA)(A)w_n, and (3) computation of the $\Delta G°$ of formation for each bound gas-phase cluster.

Initial monomer conformations were generated using the CREST conformational sampling routine in the GFN2-XTB program.[65,66] These geometries were then subjected to a series of DFT geometry optimizations using the M08-HX exchange-correlation functional and the 6−31 + G* and MG3S basis sets using the Gaussian 16 Rev. B01 program.[67−73] Finally, the electronic energy of the converged global minimum energy structures were recomputed at the domain-based local pair natural orbital coupled-cluster level with single, double, and perturbative triple excitations along with three Dunning basis sets (DLPNO-CCSD(T)/cc-pVnZ ($n = D, T, Q$))[74−83] on the M08-HX/MG3S geometries using the ORCA 4.2.1 program.[84,85] The three electronic energies were used in a 4−5 inverse polynomial complete basis set (CBS) extrapolation scheme[86] and combined with M08-HX/MG3S vibrational frequencies to calculate the thermodynamic corrections $H°$, $S°$, and $G°$ at a standard state of 1 atm pressure and temperatures of 216.65 and 298.15 K using the THERMO.pl script from the National Institute of Science and Technology.[87] The global minimum energy monomer geometries were subsequently used as input structures for a genetic-algorithm-based configurational sampling protocol to generate a wide variety of local minimum energy cluster geometries on the PM7 semiempirical potential energy surface (PES) using the OGOLEM program.[88−91] The resulting clusters were subjected to the same series of geometry optimizations and energy calculations as the monomers. ArbAlign was used to identify similar geometries with different energies.[92] The overall computational scheme is outlined in Figure 1.
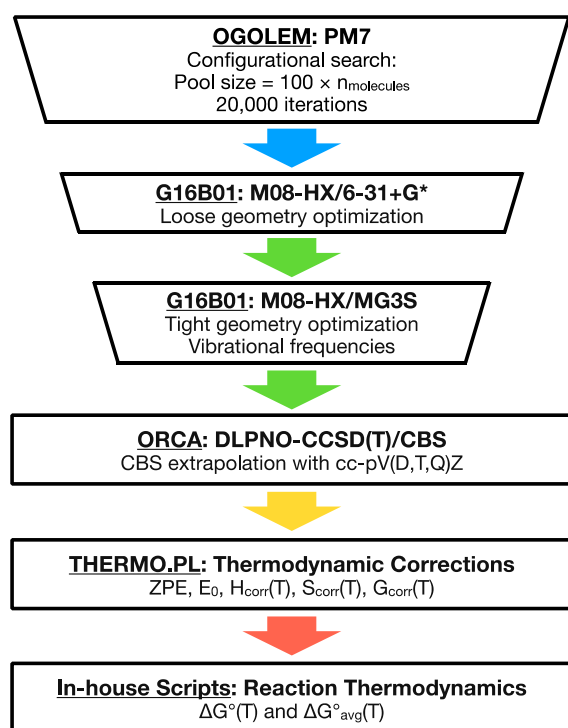
OGOLEM: PM7
Configurational search:
Pool size = 100 × $n_{molecules}$
20,000 iterations

G16B01: M08-HX/6-31+G*
Loose geometry optimization

G16B01: M08-HX/MG3S
Tight geometry optimization
Vibrational frequencies

ORCA: DLPNO-CCSD(T)/CBS
CBS extrapolation with cc-pV(D,T,Q)Z

THERMO.PL: Thermodynamic Corrections
ZPE, E_0, $H_{corr}(T)$, $S_{corr}(T)$, $G_{corr}(T)$

In-house Scripts: Reaction Thermodynamics
$\Delta G°(T)$ and $\Delta G°_{avg}(T)$

Figure 1. Computational methodology employed in this study.

It should be noted that the use of harmonic vibrational frequencies in the calculation of thermodynamic corrections presents a source of error in systems with strong anharmonic behavior, such as water clusters.[93,94] While methods such as second-order vibrational perturbation theory (VPT2)[95] and vibrational self-consistent field (VSCF)[96] do offer accurate anharmonic frequencies, the calculation of the necessary force constants becomes prohibitively expensive as the system size increases. We have recently reviewed the effects of using scaled harmonic frequencies and showed that for dry SA systems, the overall formation Gibbs free energy changes by less than 0.2 kcal mol^{-1}.[11] However, our previous MP2/CBS studies on clusters that include water have indeed shown up to 1 kcal mol^{-1} changes because of anharmonicity.[97] However, as we

describe below, errors in electronic energies far outweigh the errors in thermodynamic corrections.

An excellent review article on modeling the formation and growth of atmospheric molecular clusters details some of the key lessons learned when using quantum chemistry to explore these processes.[8] The most important factor in obtaining accurate $\Delta G°$ values is the electronic energy calculation.[8,24,27] Second, it is essential to use the appropriate symmetry numbers for the clusters because this can change the Gibbs free energy values by half a kcal mol^{-1} or more for water, ammonia, and SA.[27] Other factors, such as corrections for anharmonicity,[93,94] scaling frequencies,[9,10,97] modifying the lowest frequencies, and Boltzmann averaging the low-lying conformers, typically change the $\Delta G°$ free energy values for cluster formation by up to 1 kcal.[8,27] DFT electronic energies can sometimes have large errors, but DFT geometries are quite robust[98] with similar values for the thermal and entropic corrections for cluster formation, which makes CCSD(T)// DFT $\Delta G°$ values similar across different density functionals.[99] We have found that extrapolation to the complete basis set (CBS) limit is essential to obtain the most accurate Gibbs free energy values using MP2 and CCSD(T) methods.[9−11,24,98,100] Extrapolation using either the Riemann ζ or inverse 4−5 polynomial methods results in $\Delta G°$ values for the formation of multiple low energy clusters of $(H_2SO_4)_3$ that are 1.5−2 kcal more positive than the unextrapolated DLPNO-CCSD(T)/cc-pVTZ results.[11] The DLPNO-CCSD(T) method for electronic energies combined with DFT geometries on atmospheric molecular clusters is accurate to within a few tenths of a kcal mol^{-1} compared to the canonical CCSD(T) CBS values, at a fraction of the computational cost.[101]

The rate-limiting step in our computational methodology is the first DFT loose geometry optimization from the set of PM7 structures. Because the PM7 PES for hydrogen-bonded clusters is flat, we find that we must optimize every PM7 structure produced from the OGOLEM configurational search.[11,98] Additionally, we had to implement a cut-off in the first loose DFT geometry optimization step of 8−10 kcal mol^{-1} to ensure that we found the DLPNO-CCSD(T) free energy minimum because DFT energies are at times significantly different from CCSD(T) energies. This configurational search and initial

Table 1. DLPNO-CCSD(T)/CBS//M08-HX/MG3S Gibbs Free Energy Changes Associated with the Sequential Hydration of Sulfuric Acid, Ammonia, and Formic Acid at Temperatures of 216.65, 273.15, and 298.15 K and a Pressure of 1 atm in Units of kcal mol^{-1}

| cluster	216.65 K	273.15 K	298.65 K
$H_2SO_4 + H_2O \rightleftharpoons H_2SO_4(H_2O)$	−4.59	−2.99	−2.28
$H_2SO_4(H_2O) + H_2O \rightleftharpoons H_2SO_4(H_2O)_2$	−3.79	−2.13	−1.40
$H_2SO_4(H_2O)_2 + H_2O \rightleftharpoons H_2SO_4(H_2O)_3$	−3.39	−1.64	−0.87
$H_2SO_4(H_2O)_3 + H_2O \rightleftharpoons H_2SO_4(H_2O)_4$	−3.55	−1.88	−1.15
$H_2SO_4(H_2O)_4 + H_2O \rightleftharpoons H_2SO_4(H_2O)_5$	−1.12	0.54	1.27
$HCOOH + H_2O \rightleftharpoons HCOOH(H_2O)$	−1.36	0.39	1.16
$HCOOH(H_2O) + H_2O \rightleftharpoons HCOOH(H_2O)_2$	−2.58	−0.87	−0.11
$HCOOH(H_2O)_2 + H_2O \rightleftharpoons HCOOH(H_2O)_3$	−0.97	0.54	1.20
$HCOOH(H_2O)_3 + H_2O \rightleftharpoons HCOOH(H_2O)_4$	1.42	3.55	4.49
$HCOOH(H_2O)_4 + H_2O \rightleftharpoons HCOOH(H_2O)_5$	1.23	3.04	3.83
$NH_3 + H_2O \rightleftharpoons NH_3(H_2O)$	0.12	1.32	1.88
$NH_3(H_2O) + H_2O \rightleftharpoons NH_3(H_2O)_2$	0.00	1.83	2.63
$NH_3(H_2O)_2 + H_2O \rightleftharpoons NH_3(H_2O)_3$	−1.54	0.18	0.93
$NH_3(H_2O)_3 + H_2O \rightleftharpoons NH_3(H_2O)_4$	−0.41	1.06	1.71
$NH_3(H_2O)_4 + H_2O \rightleftharpoons NH_3(H_2O)_5$	−0.15	1.46	2.16
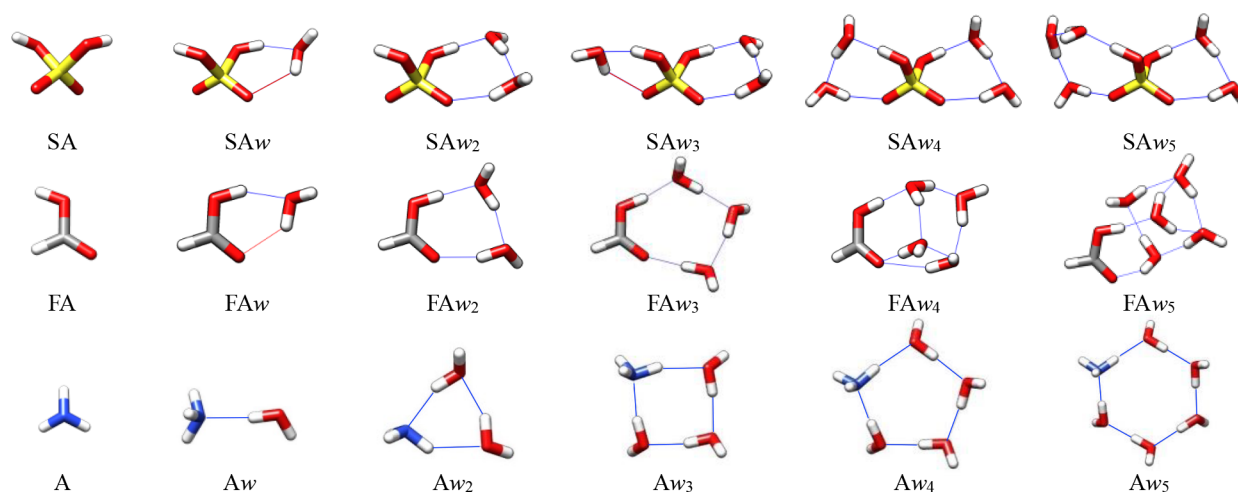
Figure 2. DLPNO-CCSD(T)/CBS//M08-HX/MG3S Gibbs free energy minima of hydrated monomer clusters, where SA is H_2SO_4, FA is HCOOH, A is NH_3, and w_n is $(H_2O)_{n = 0-5}$.

Table 2. DLPNO-CCSD(T)/CBS//M08-HX/MG3S Gibbs Free Energy Changes Associated with All Possible Hydration Reactions of Dimer Clusters at Temperatures of 216.65, 273.15, and 298.15 K and a Pressure of 1 atm in Units of kcal mol^{-1}

cluster	216.65 K	273.15 K	298.65 K
$H_2SO_4 + NH_3 \rightleftharpoons H_2SO_4(NH_3)$	−8.60	−7.01	−6.31
$H_2SO_4(NH_3) + H_2O \rightleftharpoons H_2SO_4(NH_3)(H_2O)$	−3.38	−1.67	−0.91
$H_2SO_4(NH_3)(H_2O) + H_2O \rightleftharpoons H_2SO_4(NH_3)(H_2O)_2$	−5.05	−3.11	−2.24
$H_2SO_4(NH_3)(H_2O)_2 + H_2O \rightleftharpoons H_2SO_4(NH_3)(H_2O)_3$	−3.21	−1.47	−0.79
$H_2SO_4(NH_3)(H_2O)_3 + H_2O \rightleftharpoons H_2SO_4(NH_3)(H_2O)_4$	−2.55	−0.79	0.08
$H_2SO_4(NH_3)(H_2O)_4 + H_2O \rightleftharpoons H_2SO_4(NH_3)(H_2O)_5$	−1.67	0.23	1.07
$H_2SO_4 + HCOOH \rightleftharpoons H_2SO_4(HCOOH)$	−8.49	−6.56	−5.71
$H_2SO_4(HCOOH) + H_2O \rightleftharpoons H_2SO_4(NH_3)(H_2O)$	−3.83	−2.08	−1.31
$H_2SO_4(HCOOH)(H_2O) + H_2O \rightleftharpoons H_2SO_4(HCOOH)(H_2O)_2$	−3.70	−2.00	−1.25
$H_2SO_4(HCOOH)(H_2O)_2 + H_2O \rightleftharpoons H_2SO_4(HCOOH)(H_2O)_3$	−1.56	0.01	0.70
$H_2SO_4(HCOOH)(H_2O)_3 + H_2O \rightleftharpoons H_2SO_4(HCOOH)(H_2O)_4$	−0.73	0.97	1.72
$H_2SO_4(HCOOH)(H_2O)_4 + H_2O \rightleftharpoons H_2SO_4(HCOOH)(H_2O)_5$	−0.06	2.35	3.40
$HCOOH + NH_3 \rightleftharpoons HCOOH(NH_3)$	0.51	1.91	2.53
$HCOOH(NH_3) + H_2O \rightleftharpoons HCOOH (NH_3)(H_2O)$	−5.72	−3.81	−2.96
$HCOOH(NH_3)(H_2O) + H_2O \rightleftharpoons HCOOH(NH_3)(H_2O)_2$	−0.08	1.27	1.86
$HCOOH(NH_3)(H_2O)_2 + H_2O \rightleftharpoons HCOOH(NH_3)(H_2O)_3$	0.20	2.07	2.86
$HCOOH(NH_3)(H_2O)_3 + H_2O \rightleftharpoons HCOOH(NH_3)(H_2O)_4$	−0.40	1.65	2.60
$HCOOH(NH_3)(H_2O)_4 + H_2O \rightleftharpoons HCOOH(NH_3)(H_2O)_5$	−0.38	1.42	2.21

DFT geometry optimization are crucial because failure to find the lowest energy minimum on the free energy surface (or one that is virtually the lowest) will increase the predicted $\Delta G°$ values.[8]

■ RESULTS AND DISCUSSION

FA Hydration Compared to SA and Ammonia Hydration. The sequential hydration of HCOOH as compared to H_2SO_4 and NH_3 in Table 1 lists the Gibbs free energy changes associated with the sequential hydration of these three molecules at a standard pressure of 1 atm and temperatures of 216.65, 273.15, and 298.15 K computed at the DLPNO-CCSD(T)/CBS//M08-HX/MG3S level of theory. Figure 2 shows the product geometries with hydrogen bonds displayed as blue lines (H-bond angles between 140° and 180°) and close van der Waals contacts (angles <140°) displayed as red lines. Because of its carboxyl group, HCOOH binds readily with the first three water molecules at low temperatures by forming homodromic hydrogen-bond networks in which the hydrogen bonds point in the same

direction. However, the fourth and fifth water molecules disrupt this pattern to form three-dimensional (3D) structures with less-favorable O−H−O bond angles. There are three $HCOOH(H_2O)_4$ clusters within 1 kcal mol^{-1}, the lowest of which is displayed in Figure 2. All three have water hydrogen bonding to each other. Two waters donate two hydrogen bonds to FA, and one water accepts a hydrogen bond. There are five $HCOOH(H_2O)_5$ clusters within 1 kcal mol^{-1}, the lowest of which is displayed in Figure 2, is pyramid-like, composed of a water tetramer and a formic acid−water dimer. The other three low-lying structures also have a water tetramer, and the last structure consists of a water pentamer with two of the waters bonding with FA.

NH_3 also forms homodromic hydrogen-bond networks but less-favorable N−H−O angles occur at n = 2 while favorable H-bonds occur for n = 3−5. The stabilizing effect of the stronger O−H−O hydrogen bond compared to the O−H−N and N−H−O hydrogen bonds competes with the destabilizing effect of small hydrogen-bond angles such that HCOOH-$(H_2O)_n$ is energetically more preferable at n = 1−2, and
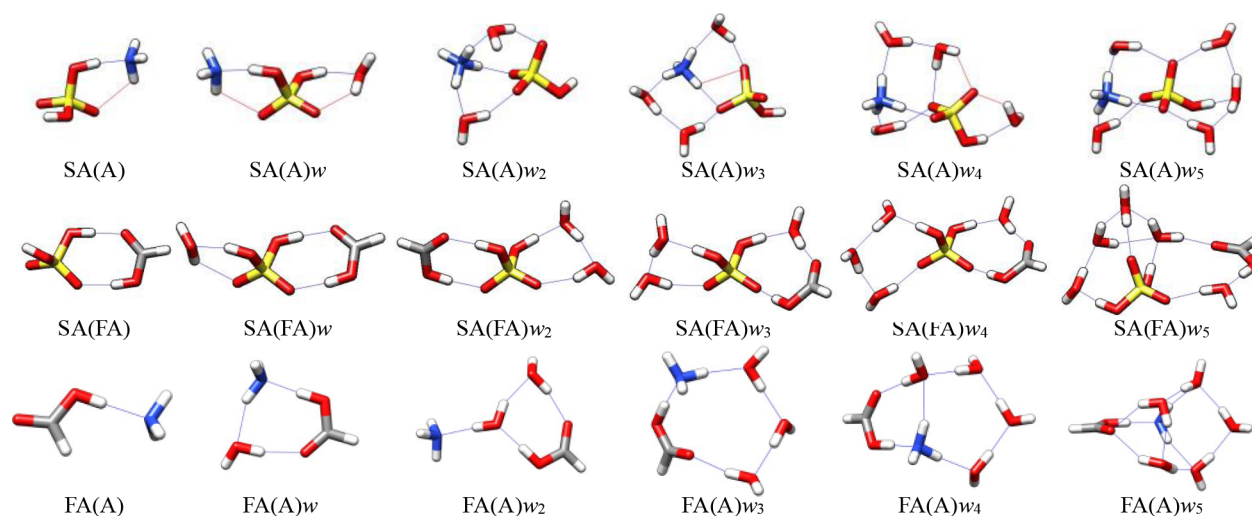
Figure 3. DLPNO-CCSD(T)/CBS//M08-HX/MG3S Gibbs free energy minima of hydrated mixed dimer clusters, where SA is H_2SO_4, FA is HCOOH, A is NH_3, and w_n is $(H_2O)_{n = 0-5}$.

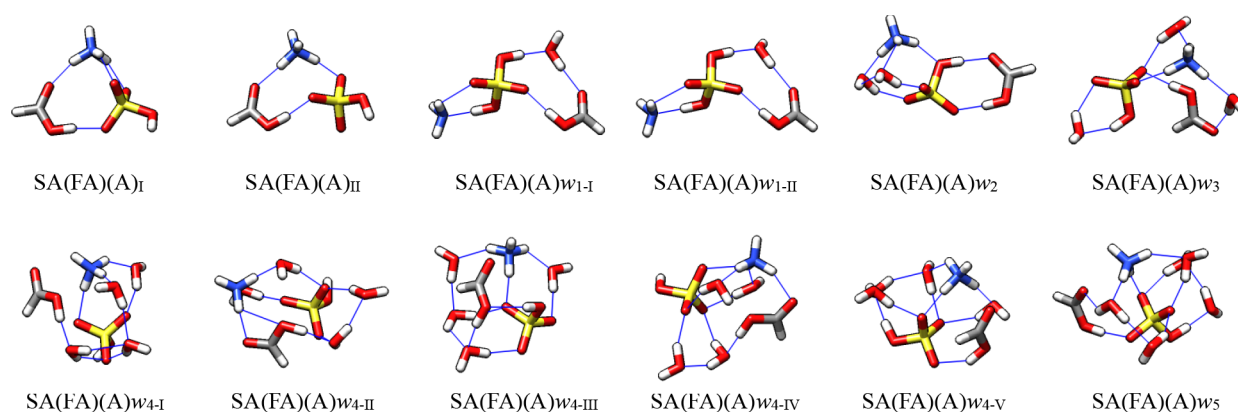**Figure 4.** DLPNO-CCSD(T)/CBS//M08-HX/MG3S Gibbs free energy minima of $H_2SO_4(HCOOH)(NH_3)(H_2O)_{n = 0-5}$, where SA is H_2SO_4, FA is HCOOH, A is NH_3, and w_n is $(H_2O)_{n = 0-5}$. Additional configurations within 1 kcal mol^{-1} of the global minima are included and marked with Roman numerals.

$NH_3(H_2O)_n$ is energetically preferable at $n = 3-5$ (Table 1). The $NH_3(H_2O)_5$ cluster has three structures within 1 kcal mol^{-1}; the cyclic structure shown in the figure and two book structures, where ammonia has replaced a water in the classic $(H_2O)_6$ book motif.

The additional carboxyl group in H_2SO_4 allows it to bind readily with water. Favorable networks form with $n = 1$ through $n = 5$. SA is a strong hydrogen-bond donor, and water is the acceptor with one or two water molecules. The waters for the $n = 1$ and 2 structures make some close contacts with the oxo oxygens. Once more waters are added, the geometries optimize such that water donates to other waters and to the oxo oxygens, while SA itself maintains strong hydrogen bonds to water.

There are six $H_2SO_4(H_2O)_2$ conformers, displaying two motifs within half a kcal mol^{-1}. The first forms a pseudo-tetramer where SA replaces two waters in the classic water tetramer, and the second has each water bridging the SA hydroxyl group and the oxo oxygen. There are five $H_2SO_4(H_2O)_3$ conformers within 1 kcal mol^{-1}, and all of them have a water dimer on one side of SA and a monomer on the other. There are two similar $H_2SO_4(H_2O)_4$ conformers within 1 kcal mol^{-1}, with a water dimer on each side of SA, as shown in the figure. The four $H_2SO_4(H_2O)_5$ structures within

1 kcal mol^{-1} have the same motif with three waters forming a pseudo-pentamer structure with the SA and two waters forming a pseudo-tetramer structure on the other side.

Hydration of Mixed Dimer Clusters. The interaction of FA with SA and ammonia in mixed dimer clusters is displayed in Table 2 and Figure 3. Table 2 lists the Gibbs free energy changes associated with the sequential hydration of sulfuric acid—ammonia, formic acid—ammonia, and sulfuric acid—FA dimers at a standard pressure of 1 atm and temperatures of 216.65, 273.15, and 298.15 K computed with DLPNO-CCSD(T)/CBS//M08-HX/MG3S. Figure 3 shows the product geometries with hydrogen bonds in red and close van der Waals contacts in blue. Comparing SA with FA, SA bonds much more strongly to ammonia than FA does, as one would expect, given the differences in acid strengths. In contrast, the formation of the $H_2SO_4(HCOOH)$ dimer is energetically competitive with the formation of the $H_2SO_4(NH_3)$ dimer stemming from the additional O—H—O hydrogen bond that HCOOH can form with H_2SO_4. Table 2 reveals that the hydration of the $H_2SO_4(HCOOH)$ dimer is energetically favorable and competitive with the hydration of $H_2SO_4(NH_3)$. This is an example of how hydrogen bonding observed in the figure, and reflected in the $\Delta G°$ values in the table, is much more important than HCOOH being a much

Table 3. DLPNO-CCSD(T)/CBS//M08-HX/MG3S Gibbs Free Energy Changes Associated with All Possible Hydration Reactions of Trimer Clusters at Temperatures of 216.65, 273.15, and 298.15 K and a Pressure of 1 atm in Units of kcal mol^{-1}

cluster	216.65 K	273.15 K	298.65 K
H_2SO_4 + HCOOH + NH_3 ⇌ $H_2SO_4(HCOOH)(NH_3)$	−17.42	−13.82	−12.23
$H_2SO_4(HCOOH)(NH_3)$ + H_2O ⇌ $H_2SO_4(HCOOH)(NH_3)(H_2O)$	−0.09	1.57	2.30
$H_2SO_4(HCOOH)(NH_3)(H_2O)$ + H_2O ⇌ $H_2SO_4(HCOOH)(NH_3)(H_2O)_2$	−3.50	−1.28	−0.30
$H_2SO_4(HCOOH)(NH_3)(H_2O)_2$ + H_2O ⇌ $H_2SO_4(HCOOH)(NH_3)(H_2O)_3$	−1.85	−0.20	0.52
$H_2SO_4(HCOOH)(NH_3)(H_2O)_3$ + H_2O ⇌ $H_2SO_4(HCOOH)(NH_3)(H_2O)_4$	−0.75	1.18	2.03
$H_2SO_4(HCOOH)(NH_3)(H_2O)_4$ + H_2O ⇌ $H_2SO_4(HCOOH)(NH_3)(H_2O)_5$	−4.45	−2.38	−1.46

weaker base than NH_3. This stems from hydrogen-bond topology and not from the traditional acid/base strength that is important at the macromolecular level.

Additionally, only the $H_2SO_4(NH_3)(H_2O)_{n\,=\,2-5}$ clusters were observed to undergo proton transfer between the acid and base molecules. The formation of an ionic system consisting of an ammonium ion and bisulfate ion occurs only in clusters with a 3D hydrogen-bond network. In contrast, the $HCOOH(NH_3)$ dimer does not undergo proton transfer and produces clusters with an overall two-dimensional (2D) hydrogen-bond network with up to four water molecules. Furthermore, the energetic stability of the $H_2SO_4(HCOOH)$ dimer clusters is comparable to the $H_2SO_4(NH_3)$ clusters *without* exhibiting proton transfer. This suggests that the stabilizing effects of the hydrogen-bond topology can be competitive with the stabilizing effects of acid−base interactions, resulting in an ionic system.

Hydration of the Mixed Sulfuric Acid−Formic Acid− Ammonia Trimer Cluster. The hydration of the mixed trimer clusters within 1 kcal mol of the minimum energy structures composed of H_2SO_4, HCOOH, and NH_3 is displayed in Figure 4. The energetics for the minimum free energy structures are in Table 3. Without waters present, SA deprotonates, and the proton is transferred to ammonia. In fact, proton transfer is observed in all clusters, except for the two $n = 1$ minima shown in Figure 4. There is only one other structure within 1 kcal mol^{-1} of the global minimum for SA(A). Structure I is the minimum, 0.68 kcal mol^{-1} lower than that of structure II on the DLPNO-CCSD(T)/CBS Gibbs free energy surface. In structure I, the ammonium cation is held strongly to the bisulfate anion much more like a salt pair and not with classical hydrogen bonds. The distances between the hydrogens on ammonium and the oxo oxygens on bisulfate are 1.85 Å, and the N−H−O bond angles are about 135°, just outside the classical hydrogen-bond angle range of 140−180°. Ammonium donates a hydrogen bond to FA (1.75 Å, 163°), and FA donates a strong hydrogen bond to bisulfate (1.65 Å, 173°). By contrast, the second structure II forms classical hydrogen bonds. In this case, ammonium donates to form two strong hydrogen bonds, one with bisulfate (1.60 Å, 166°) and one with FA (1.73 Å, 177°). FA donates to bisulfate (1.65 Å, 173°). Thus, structure I is held together by the bridging action of the ammonium to bisulfate and two hydrogen bonds, while structure II is held together by three strong hydrogen bonds.

The situation is different when one water is added to the mixture. The two lowest energy clusters are composed of neutral molecules and differ from each other by a slight rotation of the water molecule that increases the energy by 0.2 kcal mol^{-1}. Only the minimum structure for SA(FA)(A)w is displayed in Figure 4. Water bridges between SA and FA, donating a hydrogen bond to FA (1.81 Å, 169°) and accepting from SA (1.58 Å, 174°), while SA accepts a hydrogen bond

from FA (1.73 Å, 176°) and donates to ammonia (1.60 Å, 170°). The thermodynamics for adding one water to the parent cluster at standard state pressure is not favorable at higher temperatures, as observed in Table 3.

Once a second water is added to the sulfuric acid−formic acid−ammonia system, protonation returns along with more favorable free energy changes. FA and bisulfate form a strong hydrogen-bonded pair (1.67 Å, 175°; 1.71 Å, 176°); the two waters donate to the bisulfate (1.84 Å, 154°; 1.78 Å, 153°), and the ammonium donates to bisulfate (1.90 Å, 157°) and one water (1.62 Å, 168°). The addition of the second water lowers the free energy of the cluster, thus making it more favorable than the cluster with one water.

The SA(FA)(A)$w3$ minimum energy cluster is protonated, and now, ammonium donates two hydrogen bonds to two waters (1.79 Å, 177°; 1.81 Å, 157°) and one to bisulfate (1.70 Å, 171°). These two waters donate to FA (1.85 Å, 165°) and bisulfate (1.86 Å, 154°). The third water bridges the opposite side of bisulfate, accepting (1.80 Å, 156°) and donating (1.98 Å, 139°) to make more strained hydrogen bonds.

The SA(FA)(A)$w4$ system has a total of five structures within 1 kcal mol^{-1} from the global minimum. The global minimum, SA(FA)(A)$_{w4-I}$, has three waters in roughly the same plane as FA, with bisulfate and ammonium placed next to the plane, and the fourth water bridging the two ionic structures. Structure SA(FA)(A)$_{w4-II}$ is 0.31 kcal mol^{-1} higher in free energy, and this structure has two waters bridging FA and bisulfate, and the other two waters bridging ammonium and bisulfate. The next two structures ($w4$-III and $w4$-IV) are 0.65 and 0.67 kcal mol^{-1} higher in energy than $w4$-I, but with a very similar bonding motif. Structure $w4$-V is 0.88 kcal mol^{-1} above the minimum and it has all four waters bridging bisulfate and ammonium with FA donating a hydrogen bond to bisulfate on the opposite side. There is one minimum energy structure for SA(FA)(A)$w5$, and in this structure, three waters are on one side of the bisulfate-ammonium complex and the other two waters and FA are on the opposite side of the complex.

Atmospheric Implications. The $\Delta G°$ values for cluster formation shown in Tables 1−3 for the clusters presented in Figures 2−4 were used to predict the equilibrium concentrations of every possible cluster, as explained in the Methodology section. Assuming that we have a system consisting of a SA concentration of 5×10^7 cm^{-3}, equal presence of FA and ammonia of 2×10^{11} cm^{-3}, and 100% relative humidity, we calculated the equilibrium concentrations of all possible clusters in this system at 298 and 217 K. The results are displayed in Table 4 with the omission of clusters with predicted concentrations less than 1 cluster cm^{-3} at both 298 and 217 K. The concentration of clusters under these conditions is an interplay between the calculated equilibrium constants, which are larger at the top of the troposphere where

Table 4. Equilibrium Concentrations of all Clusters in Units of cm⁻³ at Temperatures of 298.15 and 216.65 K[a]

cluster	216.65 K	298.15 K
H_2SO_4	2.27×10^6	1.65×10^7
$H_2SO_4(H_2O)$	2.83×10^6	2.42×10^7
$H_2SO_4(H_2O)_2$	5.51×10^5	8.03×10^6
$H_2SO_4(H_2O)_3$	4.23×10^4	1.09×10^6
$H_2SO_4(H_2O)_4$	4.72×10^3	2.38×10^5
$H_2SO_4(H_2O)_5$	1.86	8.73×10^2
NH_3	2.00×10^{11}	2.00×10^{11}
$NH_3(H_2O)$	4.42×10^6	2.62×10^8
$NH_3(H_2O)_2$	1.29×10^2	9.67×10^4
$NH_3(H_2O)_3$	1.35×10^{-1}	6.30×10^2
$NH_3(H_2O)_4$	1.02×10^{-5}	1.10
$HCOOH$	2.00×10^{11}	1.99×10^{11}
$HCOOH(H_2O)$	1.38×10^8	8.79×10^8
$HCOOH(H_2O)_2$	1.61×10^6	3.31×10^7
$HCOOH(H_2O)_3$	4.48×10^2	1.37×10^5
$HCOOH(H_2O)_4$	4.84×10^{-4}	2.19
$H_2SO_4(NH_3)$	6.34×10^6	5.63×10^3
$H_2SO_4(NH_3)(H_2O)$	4.76×10^5	8.19×10^2
$H_2SO_4(NH_3)(H_2O)_2$	1.73×10^6	1.12×10^3
$H_2SO_4(NH_3)(H_2O)_3$	8.75×10^4	1.33×10^2
$H_2SO_4(NH_3)(H_2O)_4$	9.55×10^2	3.65
$H_2SO_4(NH_3)(H_2O)_5$	1.35	1.88×10^{-2}
$H_2SO_4(HCOOH)$	4.91×10^6	2.04×10^3
$H_2SO_4(HCOOH)(H_2O)$	1.05×10^6	5.83×10^2
$H_2SO_4(HCOOH)(H_2O)_2$	1.65×10^5	1.50×10^2
$H_2SO_4(HCOOH)(H_2O)_3$	1.81×10^2	1.44
$HCOOH(NH_3)$	3.61×10^2	2.26×10^1
$HCOOH(NH_3)(H_2O)$	6.21×10^3	1.04×10^2
$H_2SO_4(HCOOH)(NH_3)$	2.95×10^7	9.96×10^{-1}
$H_2SO_4(HCOOH)(NH_3)(H_2O)$	1.06×10^3	6.42×10^{-4}
$H_2SO_4(HCOOH)(NH_3)(H_2O)_2$	1.06×10^2	3.33×10^{-5}

[a]Initial concentration of sulfuric acid was 5×10^7 cm⁻³, formic acid and ammonia concentrations were 2×10^{11} and water concentrations were 7.7×10^{17} cm⁻³ at 298 K and 9.9×10^{14} cm⁻³ at 217 K. Concentrations less than 1 cm⁻³ at both temperatures have been omitted.

it is cooler, the concentration of water vapor, which decreases with increasing altitude, and the initial concentrations of SA, FA, and ammonia. At the bottom of the troposphere, at 100% humidity and 298 K, the simulation results predict that SA will be hydrated with 1−5 waters, while both FA and ammonia will be hydrated with 1−4 waters. The concentration of these clusters drops by one to two orders of magnitude for SA hydrates at the top of the troposphere at 217 K and by two to four orders of magnitude for FA and ammonia. In contrast, the concentrations of $H_2SO_4(NH_3)$, $H_2SO_4(HCOOH)$, and $HCOOH(NH_3)$ hydrates increase as the temperature decreases. This is because we have assumed that the concentrations of FA and ammonia are the same at both temperatures. While this assumption is probably wrong—we would expect the concentrations to decrease at lower temperature as water does—it is not clear from the experimental data what the actual concentrations of these molecules are in any region of the atmosphere. FA concentrations in the boundary layer are two to three times larger than those that can be explained by known production and loss pathways, suggesting that a large, unidentified source of FA production is missing.[43] We kept the ammonia and FA

concentrations equal and constant in our simulation in order to make comparisons, but as better estimates of the concentrations of these species are made, the $\Delta G°$ values can be used for a better estimation of the final set of clusters.

As Table 4 reveals, the concentrations of $HCOOH(NH_3)$ hydrates are much smaller than those for $H_2SO_4(NH_3)$ and $H_2SO_4(HCOOH)$ hydrates. An extremely illuminating result is that the concentrations of $H_2SO_4(NH_3)$ and $H_2SO_4(HCOOH)$ hydrated clusters are quite similar, on the order of 10^2 at 298 K and 10^2 to 10^6 cm⁻³ at 217 K. This puts the tentative prediction by Nadykto and Yu of the importance of organic acid stabilization of SA on firm ground[40] and is line with recent laboratory experiments that show that acid−base particles with mobility diameters of 5 nm are acidic.[62,63] Additionally, dry experiments of smaller clusters have shown that the basicity of the base in a sulfuric acid−base system is important.[102] While this study suggests that the basicity of alkylamine is the stabilizing factor in the formation of SA dimers, it cannot account for the effects of solvation because of experimental limitations. The hydrogen-bond topology would become much more important compared to the basicity of the amine when water molecules are added because the number of possible favorable hydrogen bonds increases drastically, and steric/geometric strains on the overall hydrogen-bond network are decreased. However, even in dry systems, the hydrogen-bond topology can be forced to play the dominant stabilizing role using functionalized amines.[103] When water is included, experimental results[103,104] agree qualitatively with our results presented here.

The $H_2SO_4(HCOOH)(NH_3)$ cluster is predicted to have a concentration of 10^7 cm⁻³ at 217 K, with significant amounts of hydration with one or two water molecules. Reducing the initial concentrations of FA and ammonia by two orders of magnitude, to 2×10^9 cm⁻³, reduces the final concentration of the $H_2SO_4(HCOOH)(NH_3)$ cluster at 217 K to 10^4 cm⁻³, and reducing the initial concentrations to 2×10^8 cm⁻³ reduces the final large cluster concentration to 10^2 cm⁻³.

◼ CONCLUSIONS

A simulation of SA, FA, ammonia, and water using highly accurate quantum chemical calculations and realistic estimates of the concentrations of these molecules in the atmosphere reveals that FA is as effective as ammonia at forming clusters with SA and water. The structure of FA is uniquely suited to form hydrogen bonds with SA, as well as partners with water to form bridges from one side of SA to the other. Hydrogen bonding topology is shown to be competitive with acid/base strength in these atmospheric prenucleation clusters. The Gibbs free energies for the formation of clusters of SA with FA and water are directly comparable to the free energies for forming sulfuric acid−ammonia−water clusters. If concentrations of FA and ammonia exceed 10^7 cm⁻³, then the sulfuric acid−formic acid−ammonia cluster is predicted to exist at the top of the troposphere and may have a role in nucleation events.

◼ ASSOCIATED CONTENT

ⓢ Supporting Information

The Supporting Information is available free of charge at https://pubs.acs.org/doi/10.1021/acs.jpca.1c10754.

> M08-HX/MG3S coordinate files of all structures within 1 kcal mol⁻¹ of the $\Delta G°$ minimum for each system,

electronic energies, G correction values, DLPNO-CCSD(T) electronic energies with the cc-pVnZ basis sets ($n = D$, T, and Q), and CBS extrapolation formula (PDF)

■ AUTHOR INFORMATION

Corresponding Author

George C. Shields − *Department of Chemistry, Furman University, Greenville, South Carolina 29613, United States;* ⊙ orcid.org/0000-0003-1287-8585; Email: george.shields@furman.edu

Authors

Shannon E. Harold − *Department of Chemistry, Furman University, Greenville, South Carolina 29613, United States*

Conor J. Bready − *Department of Chemistry, Furman University, Greenville, South Carolina 29613, United States*

Leah A. Juechter − *Department of Chemistry, Furman University, Greenville, South Carolina 29613, United States*

Luke A. Kurfman − *Department of Chemistry, Furman University, Greenville, South Carolina 29613, United States*

Sara Vanovac − *Department of Chemistry, Furman University, Greenville, South Carolina 29613, United States*

Vance R. Fowler − *Department of Chemistry, Furman University, Greenville, South Carolina 29613, United States*

Grace E. Mazaleski − *Department of Chemistry, Furman University, Greenville, South Carolina 29613, United States*

Tuguldur T. Odbadrakh − *Department of Chemistry, Furman University, Greenville, South Carolina 29613, United States*

Complete contact information is available at: https://pubs.acs.org/10.1021/acs.jpca.1c10754

Notes

The authors declare no competing financial interest.

■ REFERENCES

(1) Forster, P.; Ramaswamy, V.; Artaxo, P.; Berntsen, T.; Betts, R.; Fahey, D. W.; Haywood, J.; Lean, J.; Lowe, D. C.; Myhre, G. et al. Changes in Atmospheric Constituents and in Radiative Forcing. In *Climate Change 2007: The Physical Science Basis. Contribution of Working Group I to the Fourth Assessment Report of the Intergovernmental Panel on Climate Change*; Solomon, S.; Qin, D.; Manning, M.; Chen, Z.; Marquis, M.; Averyt, K. B.; Tignor, M.; Miller, H. L., Eds.; Cambridge University Press: Cambridge, U.K., 2007; pp 131−217.

(2) Prather, K. A.; Hatch, C. D.; Grassian, V. H. Analysis of atmospheric aerosols. *Annu. Rev. Anal. Chem.* **2008**, *1*, 485−514.

(3) Loeb, N. G.; Manalo-Smith, N. Top-of-atmosphere direct radiative effect of aerosols over global oceans from merged CERES and MODIS observations. *J. Clim.* **2005**, *18*, 3506−3526.

(4) Kallos, G.; Kushta, J.; Bartsotas, N.; Patlakas, P.; Astitha, M.; Al Qahtani, J. The Role of Aerosols in Low and Upper Atmospheric Layers Condensation. In *Air Pollution Modeling and Its Application XXIV*; Steyn, D. G., Chaumerliac, N., Eds.; N. Springer Proceedings in Complexity, 2016; pp 17−22.

(5) Nair, A. A.; Yu, F. Quantification of atmospheric ammonia concentrations: A review of its measurement and modeling. *Atmosphere* **2020**, *11*, 1092.

(6) Kerminen, V.-M.; Chen, X.; Vakkari, V.; Petäjä, T.; Kulmala, M.; Bianchi, F. Atmospheric new particle formation and growth: review of field observations. *Environ. Res. Lett.* **2018**, *13*, 103003.

(7) Smith, J. N.; Draper, D. C.; Chee, S.; Dam, M.; Glicker, H.; Myers, D.; Thomas, A. E.; Lawler, M. J.; Myllys, N. Atmospheric clusters to nanoparticles: Recent progress and challenges in closing the gap in chemical composition. *J. Aerosol Sci.* **2021**, *153*, No. 105733.

(8) Elm, J.; Kubečka, J.; Besel, V.; Jäskeläinen, M. J.; Halonen, R.; Kurtén, T.; Vehkamäki, H. Modeling the formation and growth of atmospheric molecular clusters: A review. *J. Aerosol Sci.* **2020**, *149*, No. 105621.

(9) Temelso, B.; Morrell, T. E.; Shields, R. M.; Allodi, M. A.; Wood, E. K.; Kirschner, K. N.; Castonguay, T. C.; Archer, K. A.; Shields, G. C. Quantum Mechanical Study of Sulfuric Acid Hydration: Atmospheric Implications. *J. Phys. Chem. A* **2012**, *116*, 2209−2224.

(10) Temelso, B.; Phan, T. N.; Shields, G. C. Computational study of the hydration of sulfuric acid dimers: Implications for acid dissociation and aerosol formation. *J. Phys. Chem. A* **2012**, *116*, 9745−9758.

(11) Kurfman, L. A.; Odbadrakh, T. T.; Shields, G. C. Calculating reliable Gibbs free energies for formation of gas-phase clusters that are critical for atmospheric chemistry: (H2SO4)3. *J. Phys. Chem. A* **2021**, *125*, 3169−3176.

(12) Endow, N.; Doyle, G. J.; Jones, J. L. The nature of some model photochemical aerosols. *J. Air Pollut. Control Assoc.* **1963**, *13*, 141−147.

(13) Cox, R. A.; Penkett, S. A. Aerosol formation from sulphur dioxide in the presence of ozone and olefinic hydrocarbons. *J. Chem. Soc., Faraday Trans.* **1972**, *1*, 1735−1753.

(14) Hazra, M. K.; Sinha, A. Formic acid catalyzed hydrolysis of SO3 in the gas phase: a barrierless mechanism for sulfuric acid production of potential atmospheric importance. *J. Am. Chem. Soc.* **2011**, *133*, 17444−17453.

(15) Lee, C.; Martin, R. V.; van Donkelaar, A.; Lee, H.; Dickerson, R. R.; Hains, J. C.; Krotkov, N.; Richter, A.; Vinnikov, K.; Schwab, J. J. SO2 emissions and lifetimes: Estimates from inverse modeling using in situ and global, space-based (SCIAMACHY and OMI) observations. *J. Geophys. Res.* **2011**, *116*, D06304.

(16) Li, Y.; Zhang, H.; Zhang, Q.; Xu, Y.; Nadykto, A. B. Interactions of sulfuric acid with common atmospheric bases and organic acids: Thermodynamics and implications to new particle formation. *J. Environ. Sci.* **2020**, *95*, 130−140.

(17) Zhang, R.; Khalizov, A.; Wang, L.; Hu, M.; Xu, W. Nucleation and growth of nanoparticles in the atmosphere. *Chem. Rev.* **2012**, *112*, 1957−2011.

(18) Kurten, T.; Noppel, M.; Vehkamaeki, H.; Salonen, M.; Kulmala, M. Quantum chemical studies of hydrate formation of H2SO4 and HSO4. *Boreal Environ. Res.* **2007**, *12*, 453.

(19) Loukonen, V.; Kurtén, T.; Ortega, I. K.; Vehkamäki, H.; Pádua, A. A. H.; Sellegri, K.; Kulmala, M. Enhancing Effect of Dimethylamine in Sulfuric Acid Nucleation in the Presence of Water − a Computational Study. *Atmos. Chem. Phys.* **2010**, *10*, 4961−4974.

(20) Henschel, H.; Navarro, J. C. A.; Yli-Juuti, T.; Kupiainen-Mättä, O.; Olenius, T.; Ortega, I. K.; Clegg, S. L.; Kurtén, T.; Riipinen, I.; Vehkamäki, H. Hydration of Atmospherically Relevant Molecular Clusters: Computational Chemistry and Classical Thermodynamics. *J. Phys. Chem. A* **2014**, *118*, 2599−2611.

(21) Kildgaard, J. V.; Mikkelsen, K. V.; Bilde, M.; Elm, J. Hydration of atmospheric molecular clusters: A new method for systematic configurational sampling. *J. Phys. Chem. A* **2018**, *122*, 5026−5036.

(22) Rasmussen, F. R.; Kubečka, J.; Besel, V.; Vehkamäki, H.; Mikkelsen, K. V.; Bilde, M.; Elm, J. Hydration of Atmospheric

Molecular Clusters III: Procedure for Efficient Free Energy Surface Exploration of Large Hydrated Clusters. *J. Phys. Chem. A* **2020**, *124*, 5253−5261.

(23) Hanson, D. R.; Eisele, F. L. Measurement of prenucleation molecular clusters in the NH3, H2SO4, H2O system. *J. Geophys. Res.: Atmos.* **2002**, *107*, AAC 10-1-AAC10-18.

(24) Temelso, B.; Morrison, E. F.; Speer, D. L.; Cao, B. C.; Appiah-Padi, N.; Kim, G.; Shields, G. C. Effect of mixing ammonia and alkylamines on sulfate aerosol formation. *J. Phys. Chem. A* **2018**, *122*, 1612−1622.

(25) Kurtén, T.; Torpo, L.; Ding, C.-G.; Vehkamäki, H.; Sundberg, M. R.; Laasonen, K.; Kulmala, M. A density functional study on water-sulfuric acid-ammonia clusters and implications for atmospheric cluster formation. *J. Geophys. Res.: Atmos.* **2007**, *112*, D04210.

(26) Dawson, M. L.; Varner, M. E.; Perraud, V.; Ezell, M. J.; Gerber, R. B.; Finlayson-Pitts, B. J. Simplified mechanism for new particle formation from methanesulfonic acid, amines, and water via experiments and ab initio calculations. *Proc.Natl. Acad. Sci. U. S. A.* **2012**, *109*, 18719−18724.

(27) Elm, J. Clusteromics I: Principles, Protocols, and Applications to Sulfuric Acid-Base Cluster Formation. *ACS Omega* **2021**, *6*, 7804−7814.

(28) Seinfeld, J. H.; Pandis, S. N. *Atmospheric Chemistry and Physics: From Air Pollution to Climate Change*; John Wiley & Sons, Inc.: Hoboken, New Jersey, 2016.

(29) Ortega, I. K.; Kupiainen, O.; Kurtén, T.; Olenius, T.; Wilkman, O.; McGrath, M. J.; Loukonen, V.; Vehkamäki, H. From quantum chemical formation free energies to evaporation rates. *Atmos. Chem. Phys.* **2012**, *12*, 225−235.

(30) Torpo, L.; Kurtén, T.; Vehkamäki, H.; Laasonen, K.; Sundberg, M. R.; Kulmala, M. Significance of ammonia in growth of atmospheric nanoclusters. *J. Phys. Chem. A* **2007**, *111*, 10671−10674.

(31) Kupiainen, O.; Ortega, I. K.; Kurtén, T.; Vehkamäki, H. Amine substitution into sulfuric acid – ammonia clusters. *Atmos. Chem. Phys.* **2012**, *12*, 3591−3599.

(32) Henschel, H.; Kurtén, T.; Vehkamäki, H. Computational Study on the Effect of Hydration on New Particle Formation in the Sulfuric Acid/Ammonia and Sulfuric Acid/Dimethylamine Systems. *J. Phys. Chem. A* **2016**, *120*, 1886−1896.

(33) Elm, J. Elucidating the limiting steps in sulfuric acid-base new particle formation. *J. Phys. Chem. A* **2017**, *121*, 8288−8295.

(34) Xu, Z.-Z.; Fan, H.-J. A theoretical investigation on the structures of (NH3)·(H2SO4)·(H2O)0-14 clusters. *Int. J. Quantum Chem.* **2019**, *119*, No. e25850.

(35) Leverentz, H. R.; Siepmann, J. I.; Truhlar, D. G.; Loukonen, V.; Vehkamaki, H. Energetics of atmospherically implicated clusters made of sulfuric acid, ammonia, and dimethyl amine. *J. Phys. Chem. A* **2013**, *117*, 3819−3825.

(36) Sorkin, A.; Dahlke, E. E.; Truhlar, D. G. Application of the electrostatically embedded many-body expansion to microsolvation of ammonia in water clusters. *J. Chem. Theory Comput.* **2008**, *4*, 683−688.

(37) Aloisio, S.; Hintze, P. E.; Vaida, V. The Hydration of Formic Acid. *J. Phys. Chem. A* **2002**, *106*, 363−370.

(38) Maity, D. K. How Much Water Is Needed To Ionize Formic Acid? *J. Phys. Chem. A* **2013**, *117*, 8660−8670.

(39) Zhang, R.; Jiang, S.; Liu, Y.-R.; Wen, H.; Feng, Y.-J.; Huang, T.; Huang, W. An investigation about the structures, thermodynamics and kinetics of the formic acid involved molecular clusters. *Chem. Phys.* **2018**, *507*, 44−50.

(40) Nadykto, A. B.; Yu, F. Strong hydrogen bonding between atmospheric nucleation precursors and common organics. *Chem. Phys. Lett.* **2007**, *435*, 14−18.

(41) Chen, H.; Finlayson-Pitts, B. J. New Particle Formation from Methanesulfonic Acid and Amines/Ammonia as a Function of Temperature. *Environ. Sci. Technol.* **2017**, *51*, 243−252.

(42) Puxbaum, H.; Rosenberg, C.; Gregori, M.; Lanzerstorfer, C.; Ober, E.; Winiwarter, W. Atmospheric concentrations of formic and acetic acid and related compounds in eastern and northern Austria. *Atmos. Environ.* **1988**, *22*, 2841−2850.

(43) Millet, D. B.; Baasandorj, M.; Farmer, D. K.; Thornton, J. A.; Baumann, K.; Brophy, P.; Chaliyakunnel, S.; de Gouw, J. A.; Graus, M.; Hu, L.; et al. A large and ubiquitous source of atmospheric formic acid. *Atmos. Chem. Phys.* **2015**, *15*, 6283−6304.

(44) Pan, Y.; Gu, M.; He, Y.; Wu, D.; Liu, C.; Song, L.; Tian, S.; Lü, X.; Sun, Y.; Song, T.; et al. Revisiting the concentration observations and source apportionment of atmospheric ammonia. *Adv. Atmos. Sci.* **2020**, *37*, 933−938.

(45) Chang, Y.; Zhang, Y. L.; Kawichai, S.; Wang, Q.; Van Damme, M.; Clarisse, L.; Prapamontol, T.; Lehmann, M. F. Convergent Evidence for the Pervasive but Limited Contribution of Biomass Burning to Atmospheric Ammonia in Peninsular Southeast Asia. *Atmos. Chem. Phys.* **2021**, *21*, 7187−7198.

(46) Altieri, K. E.; Spence, K. A. M.; Smith, S. Air-Sea Ammonia Fluxes Calculated From High-Resolution Summertime Observations Across the Atlantic Southern Ocean. *Geophys. Res. Lett.* **2021**, *48*, No. e2020GL091963.

(47) Kulmala, M.; Kontkanen, J.; Junninen, H.; Lehtipalo, K.; Manninen, H. E.; Nieminen, T.; Petaja, T.; Sipila, M.; Schobesberger, S.; Rantala, P.; et al. Direct observations of atmospheric aerosol nucleation. *Science* **2013**, *339*, 943−946.

(48) Almeida, J.; Schobesberger, S.; Kurten, A.; Ortega, I. K.; Kupiainen-Maatta, O.; Praplan, A. P.; Adamov, A.; Amorim, A.; Bianchi, F.; Breitenlechner, M.; et al. Molecular understanding of sulphuric acid-amine particle nucleation in the atmosphere. *Nature* **2013**, *502*, 359−363.

(49) Yu, H.; McGraw, R.; Lee, S.-H. Effects of amines on formation of sub-3 nm particles and their subsequent growth. *Geophys. Res. Lett.* **2012**, *39*, L02807.

(50) Myllys, N.; Kubečka, J.; Besel, V.; Alfaouri, D.; Olenius, T.; Smith, J. N.; Passananti, M. Role of base strength, cluster structure and charge in sulfuric-acid-driven particle formation. *Atmos. Chem. Phys.* **2019**, *19*, 9753−9768.

(51) Xie, H.-B.; Elm, J. Tri-Base Synergy in Sulfuric Acid-Base Clusters. *Atmosphere* **2021**, *12*, 1260.

(52) Vaida, V. Perspective: Water cluster mediated atmospheric chemistry. *J. Chem. Phys.* **2011**, *135*, 020901.

(53) Anglada, J. M.; Martins-Costa, M.; Ruiz-López, M. F.; Francisco, J. S. Spectroscopic signatures of ozone at the air-water interface and photochemistry implications. *Proc. Natl. Acad. Sci. U. S. A.* **2014**, *111*, 11618−11623.

(54) Zhong, J.; Kumar, M.; Francisco, J. S.; Zeng, X. C. Insight into Chemistry on Cloud/Aerosol Water Surfaces. *Acc. Chem. Res.* **2018**, *51*, 1229−1237.

(55) Zhong, J.; Kumar, M.; Anglada, J. M.; Martins-Costa, M. T. C.; Ruiz-Lopez, M. F.; Zeng, X. C.; Francisco, J. S. Atmospheric Spectroscopy and Photochemistry at Environmental Water Interfaces. *Ann. Rev. Phys. Chem.* **2019**, *70*, 45−69.

(56) Ruiz-Lopez, M. F.; Francisco, J. S.; Martins-Costa, M. T. C.; Anglada, J. M. Molecular reactions at aqueous interfaces. *Nat. Rev. Chem.* **2020**, *4*, 459−475.

(57) Liu, L.; Yu, F.; Du, L.; Yang, Z.; Francisco, J. S.; Zhang, X. Rapid sulfuric acid-dimethylamine nucleation enhanced by nitric acid in polluted regions. *Proc. Natl. Acad. Sci. U. S. A.* **2021**, *118*, No. e2108384118.
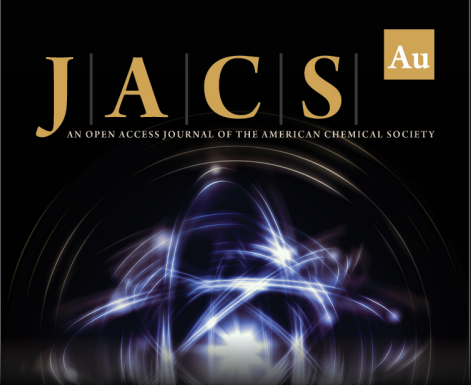
(58) Deal, A. M.; Rapf, R. J.; Vaida, V. Water-air interfaces as environments to address the Water paradox in prebiotic chemistry: A physical chemistry perspective. *J. Phys. Chem. A* **2021**, *125*, 4929−4942.

(59) Kappes, K. J.; Deal, A. M.; Jespersen, M. F.; Blair, S. L.; Doussin, J. F.; Cazaunau, M.; Pangui, E.; Hopper, B. N.; Johnson, M. S.; Vaida, V. Chemistry and photochemistry of pyruvic acid at the air-water interface. *J. Phys. Chem. A* **2021**, *125*, 1036−1049.

(60) Kreinbihl, J. J.; Frederiks, N. C.; Johnson, C. J. Hydration motifs of ammonium bisulfate clusters show complex temperature dependence. *J. Chem. Phys.* **2021**, *154*, 014304.

(61) Yang, Y.; Johnson, C. J. Hydration motifs of ammonium bisulfate clusters of relevance to atmospheric new particle formation. *Faraday Discuss.* **2019**, *217*, 47−66.

(62) Perraud, V.; Li, X.; Jiang, J.; Finlayson-Pitts, B. J.; Smith, J. N. Size-Resolved Chemical Composition of Sub-20 nm Particles from Methanesulfonic Acid Reactions with Methylamine and Ammonia. *ACS Earth Space Chem.* **2020**, *4*, 1182−1194.

(63) Chen, H.; Chee, S.; Lawler, M. J.; Barsanti, K. C.; Wong, B. M.; Smith, J. N. Size resolved chemical composition of nanoparticles from reactions of sulfuric acid with ammonia and dimethylamine. *Aerosol Sci. Technol.* **2018**, *52*, 1120−1133.

(64) Odbadrakh, T. T.; Gale, A. G.; Ball, B. T.; Temelso, B.; Shields, G. C. Computation of atmospheric concentrations of molecular clusters from ab initio thermochemistry. *J. Visualized Exp.* **2020**, *158*, No. e60964.

(65) Grimme, S. Exploration of chemical compound, conformer, and reaction space with meta- dynamics simulations based on tight-binding quantum chemical calculations. *J. Chem. Theory Comput.* **2019**, *15*, 2847−2862.

(66) Bannwarth, C.; Ehlert, S.; Grimme, S. GFN2-xTB-An accurate and broadly parametrized self- consistent tight-binding quantum chemical method with multipole electrostatics and density-dependent dispersion contributions. *J. Chem. Theory Comput.* **2019**, *15*, 1652−1671.

(67) Zhao, Y.; Truhlar, D. G. Exploring the limit of accuracy of the global hybrid meta density functional for main-group thermochemistry, kinetics, and noncovalent interactions. *J. Chem. Theory Comput.* **2008**, *4*, 1849−1868.

(68) Ditchfield, R.; Hehre, W. J.; Pople, J. A. Self-consistent molecular-orbital methods. IX. An extended Gaussian-type basis for molecular-orbital studies of organic molecules. *J. Chem. Phys.* **1971**, *54*, 724−728.

(69) Hehre, W. J.; Ditchfield, R.; Pople, J. A. Self-consistent molecular orbital methods 12. Further extensions of Gaussian-type sets for use in molecular-orbital studies of organic molecules. *J. Chem. Phys.* **1972**, *56*, 2257−2261.

(70) Krishnan, R.; Binkley, J. S.; Seeger, R.; Pople, J. A. Self-consistent molecular orbital methods. XX. A basis set for correlated wave functions. *J. Chem. Phys.* **1980**, *72*, 650−654.

(71) Frisch, M. J.; Pople, J. A.; Binkley, J. S. Self-consistent molecular orbital methods 25. Supplementary functions for Gaussian basis sets. *J. Chem. Phys.* **1984**, *80*, 3265−3269.

(72) Clark, T.; Chandrasekhar, J.; Spitznagel, G. W.; Schleyer, P. V. R. Efficient diffuse function-augmented basis sets for anion calculations. III. The 3-21+G basis set for first-row elements, Li-F. *J. Comput. Chem.* **1983**, *4*, 294−301.

(73) Frisch, M. J.; Trucks, G. W.; Schlegel, H. B.; Scuseria, G. E.; Robb, M. A.; Cheeseman, J. R.; Scalmani, G.; Barone, V.; Petersson, G. A.; Nakatsuji, H. et al. *Gaussian 16 Rev. B.01*; Wallingford, CT, 2016.

(74) Neese, F. Prediction of molecular properties and molecular spectroscopy with density functional theory: From fundamental theory to exchange-coupling. *Coord. Chem. Rev.* **2009**, *253*, 526−563.

(75) Neese, F.; Wennmohs, F.; Hansen, A. Efficient and accurate local approximations to coupled-electron pair approaches: An attempt to revive the pair natural orbital method. *J. Chem. Phys.* **2009**, *130*, 114108.

(76) Neese, F.; Hansen, A.; Liakos, D. G. Efficient and accurate approximations to the local coupled cluster singles doubles method using a truncated pair natural orbital basis. *J. Chem. Phys.* **2009**, *131*, 064103.

(77) Hansen, A.; Liakos, D. G.; Neese, F. Efficient and accurate local single reference correlation methods for high-spin open-shell molecules using pair natural orbitals. *J. Chem. Phys.* **2011**, *135*, 214102.

(78) Riplinger, C.; Neese, F. An efficient and near linear scaling pair natural orbital based local coupled cluster method. *J. Chem. Phys.* **2013**, *138*, 034106.

(79) Liakos, D. G.; Sparta, M.; Kesharwani, M. K.; Martin, J. M.; Neese, F. Exploring the accuracy limits of local pair natural orbital coupled-cluster theory. *J. Chem. Theory Comput.* **2015**, *11*, 1525−1539.

(80) Liakos, D. G.; Neese, F. Is it possible to obtain coupled cluster quality energies at near density functional theory cost? Domain-based local pair natural orbital coupled cluster vs modern density functional theory. *J. Chem. Theory Comput.* **2015**, *11*, 4054−4063.

(81) Riplinger, C.; Pinski, P.; Becker, U.; Valeev, E. F.; Neese, F. SparseMaps − A systematic infrastructure for reduced-scaling electronic structure methods. II. Linear scaling domain based pair natural orbital coupled cluster theory. *J. Chem. Phys.* **2016**, *144*, 024109.

(82) Pavosevic, F.; Peng, C.; Pinski, P.; Riplinger, C.; Neese, F.; Valeev, E. F. SparseMaps − A systematic infrastructure for reduced scaling electronic structure methods. V. Linear scaling explicitly correlated coupled-cluster method with pair natural orbitals. *J. Chem. Phys.* **2017**, *146*, 174108.

(83) Guo, Y.; Riplinger, C.; Becker, U.; Liakos, D. G.; Minenkov, Y.; Cavallo, L.; Neese, F. Communication: An improved linear scaling perturbative triples correction for the domain based local pair-natural orbital based singles and doubles coupled cluster method [DLPNO-CCSD(T)]. *J. Chem. Phys.* **2018**, *148*, 011101.

(84) Neese, F. The ORCA program system. *Wiley Interdiscip. Rev.: Comput. Mol. Sci.* **2012**, *2*, 73−78.

(85) Neese, F. Software update: the ORCA program system, version 4.0. *Wiley Interdiscip. Rev.: Comput. Mol. Sci.* **2017**, *8*, e1327.

(86) Helgaker, T.; Klopper, W.; Koch, H.; Noga, J. Basis-set convergence of correlated calculations on water. *J. Chem. Phys.* **1997**, *106*, 9639−9646.

(87) Irikura, K. K. *THERMO.PL*; National Institute of Standards and Technology, 2002.

(88) Hostaš, J.; Řezáč, J.; Hobza, P. On the performance of the semiempirical quantum mechanical PM6 and PM7 methods for noncovalent interactions. *Chem. Phys. Lett.* **2013**, *568−569*, 161−166.

(89) Stewart, J. J. P. An investigation into the applicability of the semiempirical method PM7 for modeling the catalytic mechanism in the enzyme chymotrypsin. *J. Mol. Model.* **2017**, *23*, 154.

(90) Dieterich, J. M.; Hartke, B. OGOLEM: Global cluster structure optimisation for arbitrary mixtures of flexible molecules. A multi-scaling, object-oriented approach. *Mol. Phys.* **2010**, *108*, 279−291.

(91) Hartke, B. Global optimization. *Wiley Interdiscip. Rev.: Comput. Mol. Sci.* **2011**, *1*, 879−887.

(92) Temelso, B.; Mabey, J. M.; Kubota, T.; Appiah-Padi, N.; Shields, G. C. ArbAlign: A tool for optimal alignment of arbitrarily ordered isomers using the Kuhn-Munkres Algorithm. *J. Chem. Theory Comput.* **2017**, *57*, 1045−1054.

(93) Temelso, B.; Archer, K. A.; Shields, G. C. Benchmark structures and binding energies of small water clusters with anharmonicity corrections. *J. Phys. Chem. A* **2011**, *115*, 12034−12046.

(94) Temelso, B.; Shields, G. C. The role of anharmonicity in hydrogen-bonded systems: The case of water clusters. *J. Chem. Theory Comput.* **2011**, *7*, 2804−2817.

(95) Barone, V. Anharmonic vibrational properties by a fully automated second-order perturbative approach. *J. Chem. Phys.* **2005**, *122*, 14108.

(96) Hansen, M. B.; Sparta, M.; Seidler, P.; Toffoli, D.; Christiansen, O. New formulation and implementation of vibrational self-consistent field theory. *J. Chem. Theory Comput.* **2010**, *6*, 235−248.

(97) Bustos, D. J.; Temelso, B.; Shields, G. C. Hydration of the sulfuric acid-methylamine complex and implications for aerosol formation. *J. Phys. Chem. A* **2014**, *118*, 7430−7441.

(98) Ball, B. T.; Vanovac, S.; Odbadrakh, T. T.; Shields, G. C. Monomers of Glycine and Serine Have a Limited Ability to Hydrate in the Atmosphere. *J. Phys. Chem. A* **2021**, *125*, 8454−8467.

(99) Elm, J.; Mikkelsen, K. V. Computational approaches for efficiently modelling of small atmospheric clusters. *Chem. Phys. Lett.* **2014**, *615*, 26−29.

(100) Morrell, T. E.; Shields, G. C. Atmospheric Implications for Formation of Clusters of Ammonium and 1-10 Water Molecules. *J. Phys. Chem. A* **2010**, *114*, 4266−4271.

(101) Schmitz, G.; Elm, J. Assessment of the DLPNO Binding Energies of Strongly Noncovalent Bonded Atmospheric Molecular Clusters. *ACS Omega* **2020**, *5*, 7601−7612.

(102) Jen, C. N.; McMurry, P. H.; Hanson, D. R. Stabilization of sulfuric acid dimers by ammonia, methylamine, dimethylamine, and trimethylamine. *J. Geophys. Res.: Atmos.* **2014**, *119*, 7502−7514.

(103) Waller, S. E.; Yang, Y.; Castracane, E.; Racow, E. E.; Kreinbihl, J. J.; Nickson, K. A.; Johnson, C. J. The interplay between hydrogen bonding and Coulombic forces in determining the structure of sulfuric acid-amine clusters. *J. Phys. Chem. Lett.* **2018**, *9*, 1216−1222.

(104) Thomas, J. M.; He, S.; Larriba-Andaluz, C.; DePalma, J. W.; Johnston, M. V.; Hogan, C. J., Jr. Ion mobility spectrometry-mass spectrometry examination of the structures, stabilities, and extents of hydration of dimethylamine-sulfuric acid clusters. *Phys. Chem. Chem. Phys.* **2016**, *18*, 22962−22972.

(105) Shields, G. C. Twenty years of exceptional success: The molecular education and research consortium in undergraduate computational chemistry (MERCURY). *Int. J. Quantum Chem.* **2020**, *120*, e26274.